

Exploring AMR Sensors' Performance Limits Using an Agile, High-Speed Set–Reset Pulse Generation Circuit

Neoclis Hadjigeorgiou^{ID}, Konstantinos Papafotis^{ID}, and Paul P. Sotiriadis^{ID}

Department of Electrical and Computer Engineering, National Technical University of Athens, 15780 Athens, Greece

This work explores the performance characteristics of anisotropic magnetoresistance (AMR) sensors when operating with very short set/reset current polarization pulses. AMR sensor's sensitivity, offset, and power consumption are measured and reported using the sequences of set/reset polarization pulses of different durations. In order to perform these measurements, a circuit topology for generating agile current pulses with variable duration down to 40 ns, i.e., about fifty times shorter than similar circuits reported in the literature, was devised. It is demonstrated that AMR sensors maintain their sensitivity and offset even with polarization pulses two orders of magnitude shorter than those recommended in the literature. This allows for the faster magnetic field sampling and the lower power consumption which can significantly broaden the application space of AMR sensors.

Index Terms—Anisotropic magnetoresistance (AMR), offset, pulse generation circuit, sensitivity, set–reset, set–reset circuit.

I. INTRODUCTION

ANISOTROPIC magnetoresistance (AMR) magnetic sensors are built around sensing elements which typically consist of four anisotropic magnetoresistors in a Wheatstone bridge configuration. The magnetoresistors are formed out of thin-film strips made up of patterned Ni–Fe permalloy in a barber-pole configuration [1]–[3]. The structure of a typical AMR sensing element is shown in Fig. 1.

Although the AMR Wheatstone bridge sensing element may have a better sensitivity than other magnetic sensing elements [3]–[6], it comes with certain nonidealities that need to be addressed in the design of a quality (high-sensitivity, accurate, wide-bandwidth, and reliable) sensor.

- 1) Offset voltage (output in the absence of magnetic field), caused by mismatches due to manufacturing imperfections, which is temperature dependent [3]–[9].
- 2) Sensitivity temperature dependence [3]–[6] and sensitivity degradation when it is exposed to high intensity magnetic field [6]–[9].
- 3) Hysteresis (memory effect) [3]–[10] and static nonlinearity [5].
- 4) Crossfield, i.e., the unwanted nonlinear sensitivity to fields perpendicular to the desired sensing direction [6], [11]–[13], common to sensors using ferromagnetic materials [1], [3]–[5].

To alleviate these non-idealities, high sensitivity AMR sensors include two coils inductively coupled to the sensing element: the set/reset (S/R) coil and the offset (feedback) coil as shown in Fig. 2 [9]. Applying current to the S/R coil generates a magnetic field in the *easy* magnetization axis of the ferromagnetic material of the sensing element, whereas

Manuscript received January 16, 2020; revised April 8, 2020; accepted June 25, 2020. Date of publication July 17, 2020; date of current version August 20, 2020. Corresponding author: N. Hadjigeorgiou (e-mail: neoklis@teamkb.com).

Color versions of one or more of the figures in this article are available online at <http://ieeexplore.ieee.org>.

Digital Object Identifier 10.1109/TMAG.2020.3009870

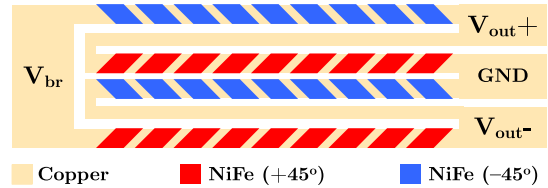


Fig. 1. Typical structure of AMR sensing element.

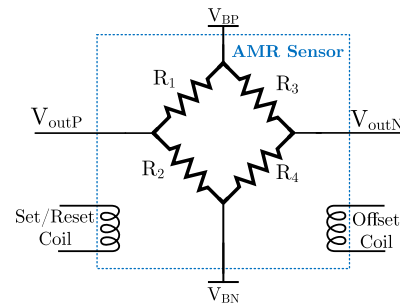


Fig. 2. Functional model of an AMR sensor with offset and set/reset coils.

applying current to the offset coil generates a magnetic field in the hard (sensing) axis.

Offset, hysteresis, and crossfield nonidealities can be eliminated, in principle, by alternating polarization (flipping the magnetic domains) of the sensing element and double measurements [5]–[9], [14]–[18]. That is, a positive current pulse passes through the S/R coil (set) to polarize the element positively, and then, a first measurement is done; next, a negative current pulse passes through the S/R coil (reset) to polarize it negatively, and after that, a second measurement is done. The difference between the two measurements is the output of the magnetic field measurement, and the whole pattern can be repeated periodically.

Sensitivity variation and static nonlinearity can be eliminated by operating the AMR sensor in a high-gain closed loop.

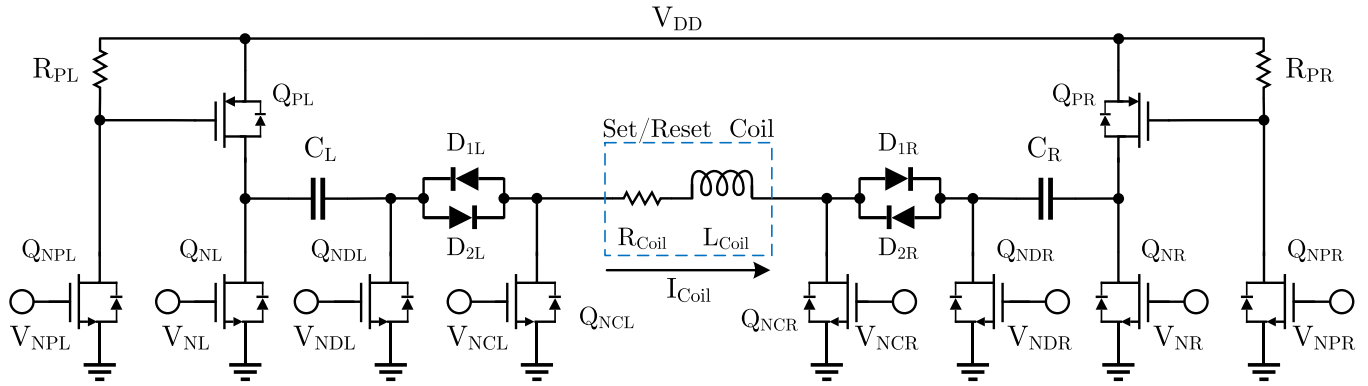


Fig. 3. Proposed set/reset pulse generation circuit.

This can be done by feeding the magnetic field generated by the offset coil back to the sensing element [5], [19]–[22].

The application of the aforementioned dual polarization and measurement and feedback strategy to eliminate the nonidealities of the AMR sensing element introduces the following challenges. First of all, a circuit is needed to provide the set and the reset high current pulses to the S/R coil, and the pulses must be complementary to avoid biasing. Furthermore, assuming that the dual polarization and measurement pattern is repeated indefinitely with repetition frequency f , for continuous measurement of the magnetic field, then one needs to consider the duration of the current pulses, T_P .

It is desirable to have T_P as small as possible¹ for at least three reasons: The first one is to allow for as high f as possible. The second one is to minimize the power consumption of the total sensor system, especially for portable battery-powered applications. The third one is to minimize power dissipation on the package of sensors which is converted to heat, raising its temperature and altering the properties of the sensing elements.

Note that measurements cannot be done during the set and reset pulses; therefore, from the total period $1/f$ of the pattern, $2T_P$ is lost. Moreover, since the magnetic field is essentially *sampled* at a frequency rate of f , the Nyquist sampling theorem states that any magnetic field frequency component above $f/2$ (in practice $f/3$ or even lower) will result in aliasing and corrupted measurements [23]. Therefore, the high value of f is desirable in several applications, especially when the sensor operates in a closed loop [22]–[24], and its actual bandwidth must be at least one order of magnitude less than f . This is why a fast and agile S/R pulse circuit is necessary to provide short current pulses.

Commercially available high-resolution AMR sensors do not include an electronic circuit to pulse the S/R coil. Most of the users (see [19]–[21], [25], [26]) implement basic circuit topologies provided in the manufacturer's datasheet and application notes [9]. S/R pulse duration T_P in a typical sensor's application is a few microseconds although the intrinsic operating bandwidth of the sensing element is several

¹However, sufficiently large to allow the magnetic dipoles to flip, which depends on the material and size. Typical values are a few tens of nanoseconds.

megahertz [9]. Thus, basic pulse generation circuits are not designed to provide short-duration current pulses that are required to operate the sensor in higher frequencies and utilize their large bandwidth.

The purpose of this work is threefold: 1) to propose a circuit topology capable of generating agile current pulses with variable duration T_P down to 40 ns, i.e., about fifty times shorter than similar circuits reported in the literature; 2) to explore the performance limits of an AMR sensor when it operates with very short S/R pulses. Specifically, we use the proposed circuit to demonstrate that the sensitivity and offset of an AMR sensor HMC100X by Honeywell are not degraded even when using 40 ns S/R pulses. Note that the magnetic material of the sensor (Ni-Fe permalloy) can operate using much shorter S/R pulses. However, by inspecting the sensor's (chip) model [28] and capturing its internal parasitics, it becomes evident that the (complete) sensor is not designed to operate with very short S/R pulses whose harmonic content extends to much high frequencies; and 3) to evaluate the thermal response of the examined AMR sensor to periodic S/R sequences with variable pulse duration and to experimentally derive the package-to-ambient thermal resistance.

This article is organized into four sections. In Section II, the proposed circuit for the S/R pulses generation is presented. The sensor's transient and steady-state response to S/R pulses of different duration are shown in Section III. In Section IV, power consumption and temperature of the sensor when it operates under S/R pulses of different duration are presented. Finally, conclusions are discussed in Section V.

II. THE SET-RESET PULSE CIRCUIT ARCHITECTURE

For the generation of the S/R pulses, we propose the circuit architecture in Fig. 3. It is capable of generating agile, very short current pulses with variable duration down to 40 ns, achieving fine pulse control for high-speed applications. In addition, the generated set and reset pulses are symmetrical due to the fully differential architecture of the circuit.

A. Circuit and Timing Description

The proposed circuit is a modified H-bridge [27] with a capacitive coupling to the load S/R Coil and two sets of

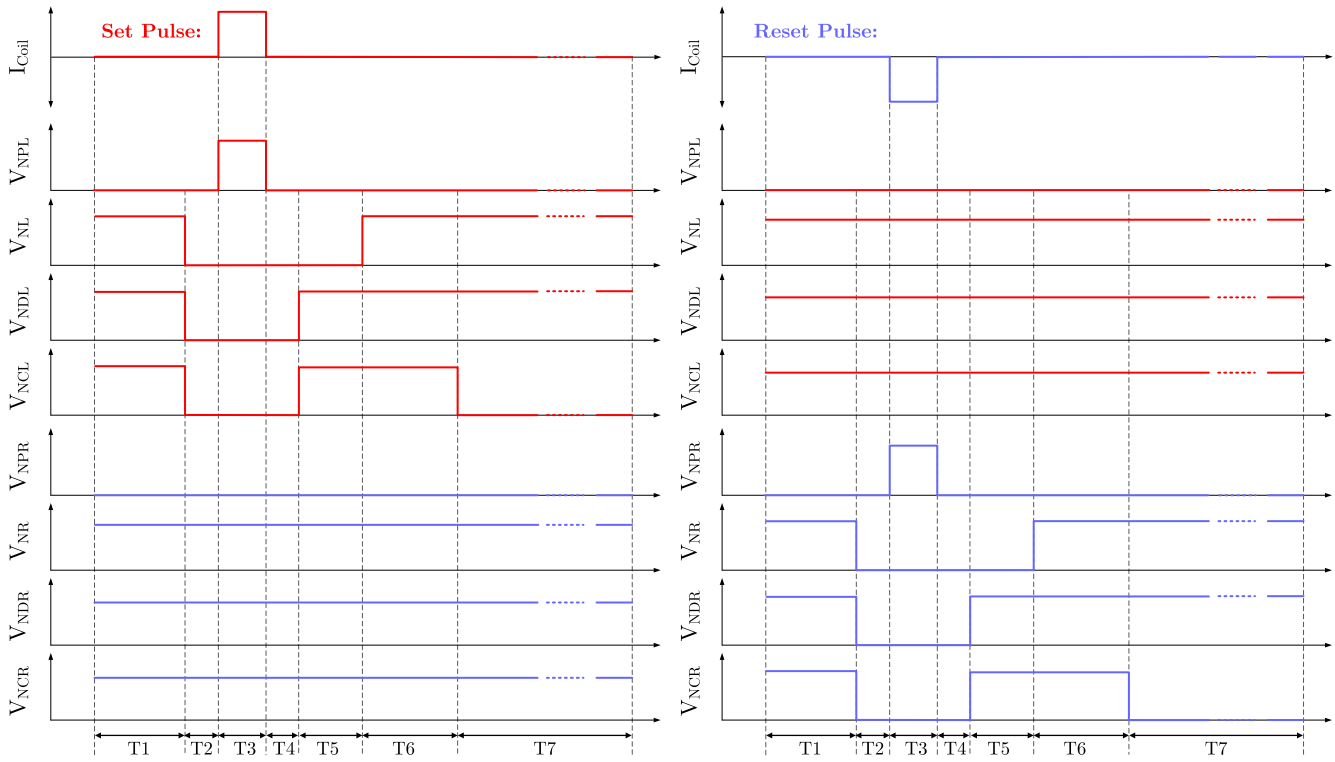


Fig. 4. Control signals' sequence for generating set and reset pulses.

dead-band generating diodes. Although a simple H-bridge (e.g., Q_{NPL} , R_{PL} , Q_{PL} , Q_{NL} , Q_{NPR} , R_{PR} , Q_{PR} , and Q_{NR}) can be sufficient for certain S/R patterns, the proposed circuit is more versatile allowing for different S/R patterns and strategies for experimentation.²

The digital signals controlling the gates of the MOSFET transistors are shown in Fig. 4 over the complete set-and-measure and reset-and-measure time intervals. Set–reset takes place during the time intervals T1–T6, whereas measurement (or multiple measurements) takes place during time interval T7. Note that time interval T7 may be omitted if a set/reset sequence (T1, T2, . . . , T6) is followed by another S/R sequence before the next measurement.

The MOSFET transistors operate in ON/OFF mode, as switches, resulting in different configurations according to the control signals. Since the circuit and the signaling are fully balanced, it is sufficient to discuss its operation during the complete set-and-measure interval since the reset-and-measure one is exactly complementary.

²Specifically: 1) capacitors C_L and C_R are added to block dc current, possibly damaging the S/R coil, in case of timing errors; 2) since C_L and C_R are charged during S/R, to remove memory effects from one S/R phase to the next (energy stored in C_L and C_R), transistors Q_{NDL} and Q_{NDR} are added to controllably short-circuit C_L and C_R and zero their voltage; 3) to allow the option to open circuit the S/R coil and eliminate the possible inductive current due to its parasitic coupling with the feedback coil [28], diodes $D_{(1,2)L}$ and $D_{(1,2)R}$ are added in series with the S/R coil offering very high small-signal resistance in zero dc bias; and 4) finally, transistors Q_{NCL} and Q_{NCR} are added to allow short-circuiting coil in order to zero its stored magnetic field energy.

The configurations of the circuit during the seven set-and-measure intervals are shown in Fig. 5, and its operation is explained as follows.

- T1: During T1, the capacitor C_L is fully discharged, and the S/R coil is short circuited. This is done with transistors Q_{NL} , Q_{NDL} , Q_{NCL} , Q_{NR} , Q_{NDR} , and Q_{NCR} conducting while all other ones are in the cutoff. The corresponding configuration is shown in Fig. 5(a).
- T2: This is an overlap protection period. Transistors such as Q_{NL} , Q_{NDL} , and Q_{NCL} are turned off to avoid any short-circuit current when Q_{PL} turns on in T3. The corresponding configuration is shown in Fig. 5(b).
- T3: The set current pulse is generated. Transistor Q_{NPL} is turned on which consequently turns on Q_{PL} . Current flows through the path of Q_{PL} , C_L , and D_{2L} and the S/R coil to ground through the closed Q_{NCR} . The last one must have small r_{ON} to avoid any essential current flows through the anti-parallel diodes D_{1R} and D_{2R} . At the end of T3, Q_{PL} is turned off zeroing the current to the S/R coil through D_{2L} . The corresponding configuration is shown in Fig. 5(c). During T3, the magnetic domains of the sensor element are turned into the set state by the strong magnetic field created by the current through the S/R coil.
- T4: This is an overlap protection period like T2. Transistors Q_{NDL} and Q_{NCL} remain off, before they are turned on during T5, to avoid short-circuit current through Q_{PL} which is turning off (via C_L). S/R coil current continuity implies that, at the beginning of T4, the drain voltage of Q_{NCL} may become negative (depending on

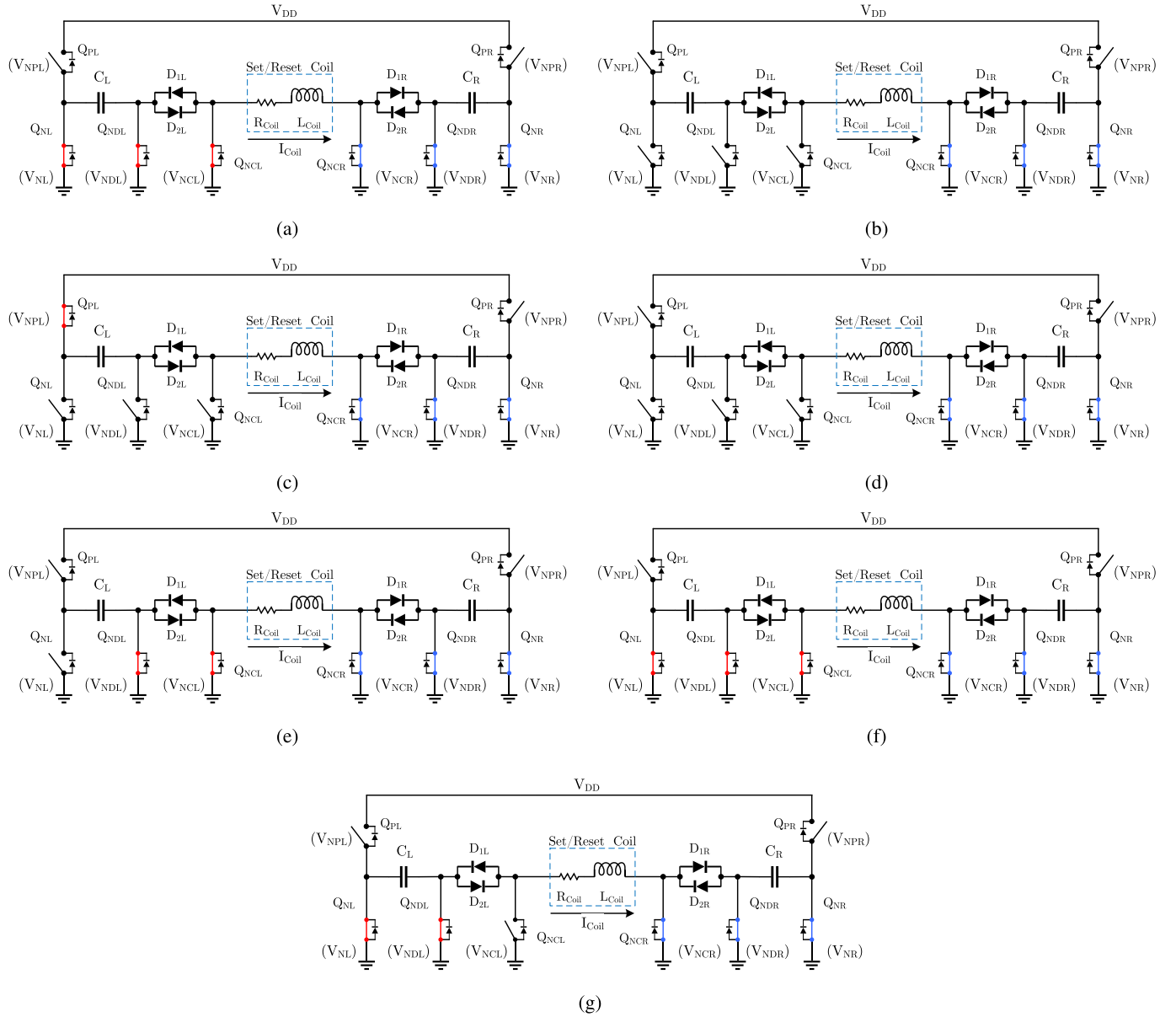


Fig. 5. Configuration of transistor switches during T1–T7. (a) Interval 1. (b) Interval 2. (c) Interval 3. (d) Interval 4. (e) Interval 5. (f) Interval 6. (g) Interval 7.

parasitic capacitance), and the energy stored in the coil is discharged through the internal diode of Q_{NCL} . The corresponding configuration is shown in Fig. 5(d).

T5: The S/R coil is discharged through transistor Q_{NCL} which is turned on along with transistors Q_{NDL} . The corresponding configuration is shown in Fig. 5(e).

T6: The transistor Q_{NL} is turned on, and the capacitor C_L is fully discharged through Q_{NL} and Q_{NDL} . Furthermore, during T6 (and partially during T5), the magnetic domains of the sensor elements are stabilized into the set state. The corresponding configuration is shown in Fig. 5(f).

T7: This is the measurement interval. Transistors Q_{NL} and Q_{NDL} are on to keep C_L short circuited. Furthermore, transistor Q_{NCL} is cutoff, whereas Q_{NCR} is on. This results in a grounded right side of the S/R coil and zero dc-biased diodes D_{1L} and D_{2L} , which leaves the

left side of the S/R coil essentially unconnected. This is important in order to avoid current through the S/R coil, caused by induced voltage due to the external magnetic field or due to the parasitic inductive coupling between the S/R coil and the offset coil [28]. The corresponding configuration is shown in Fig. 5(g).

B. Measurements and Waveforms

To demonstrate the operation and the timing of the proposed circuit in Fig. 3, two experiments were performed.

- 1) A sequence of control signals for producing a 1 μ s reset pulse was generated and captured by an oscilloscope. The measured waveforms are shown in Fig. 6.
- 2) The current through the S/R coil for both set and reset pulses of different durations was recorded by the oscilloscope, and it is shown in Fig. 7.

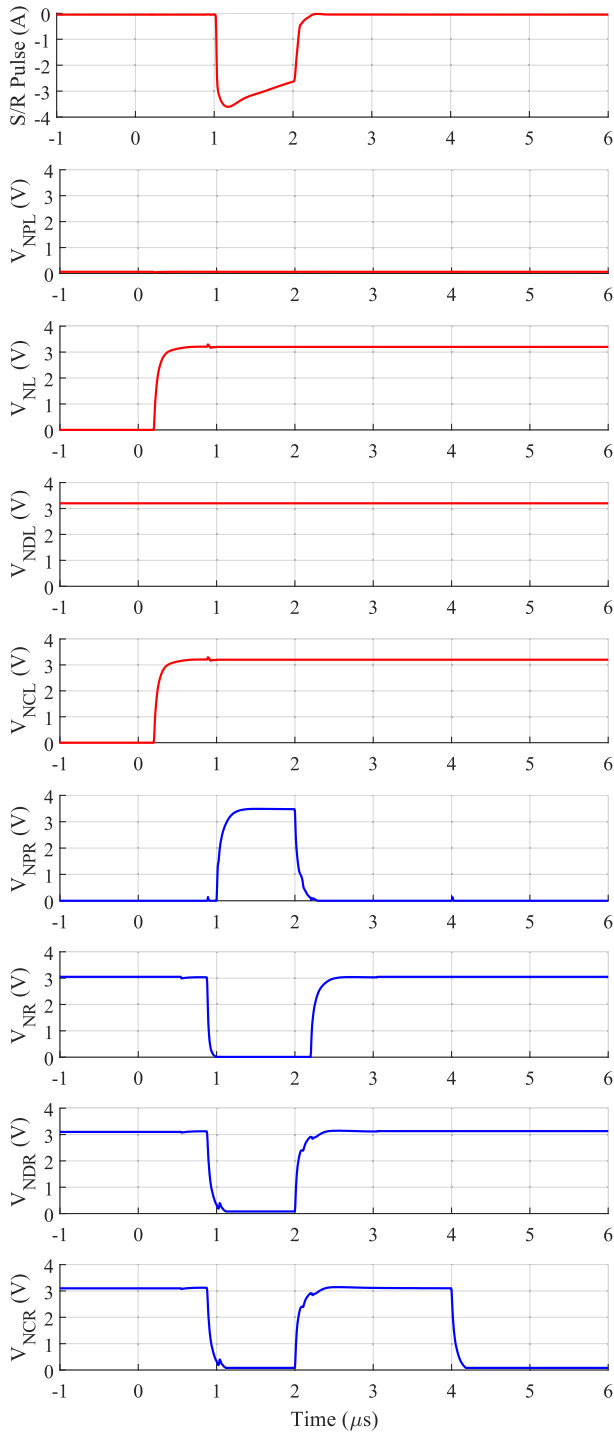


Fig. 6. Sequence of control signals for 1 μ s reset pulse.

In both cases, the S/R coil current was measured by inserting an 0.1Ω resistor in series with the coil.

The slope (non-flatness) of the ideally square current pulse, during their on time, is caused by the charging of the protective capacitors C_L and C_R due to their relatively small size, and it is eliminated if the capacitors are removed.

Finally, as shown in Fig. 7, the proposed circuit is capable of generating sharp current pulses with variable duration down to 40 ns. The rise time of the pulses in Fig. 7 is about

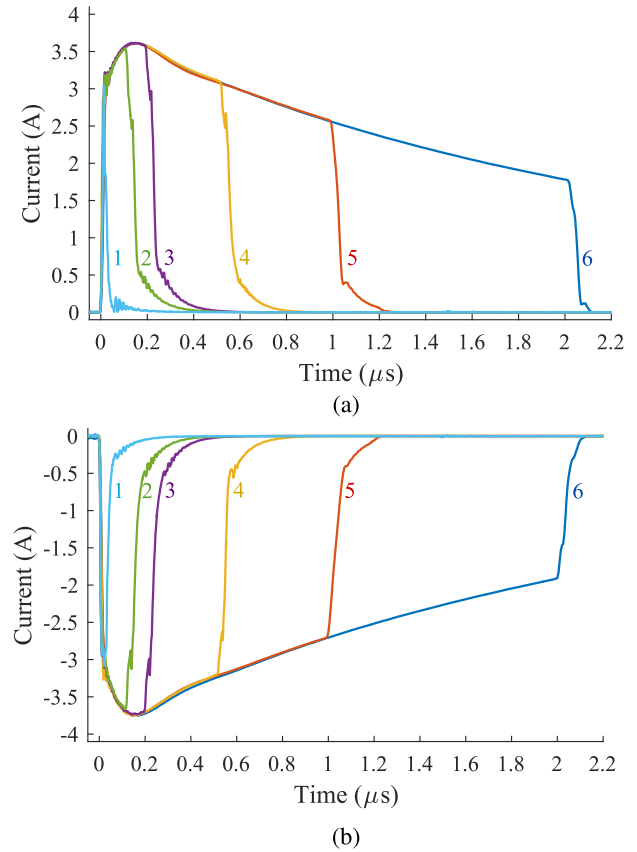


Fig. 7. Different current pulses for (a) set and (b) reset of 40 ns (cyan), 200 ns (green), 300 ns (purple), 600 ns (yellow), 1 μ s (orange), and 2 μ s (blue) duration.

20 ns. The set and reset pulses are symmetrical due to the fully differential architecture of the circuit.

C. Circuit Implementation Considerations

The certain aspects of the circuit in Fig. 3 must be taken into consideration in order for it to operate correctly and fast in the nanosecond time scale.

The MOSFET transistors operate as on/off switches, driven by the control signal sequences. Therefore, it is important that their r_{ON} resistance is small, and their turn-on and turn-off times are small. The transistors must be placed close to the S/R coil to minimize any additional parasitic resistance and inductance.

Moreover, the transistors must have appropriate threshold voltage and small input capacitance and gate charge, Q_g . This is crucial for them to switch fast when driven directly by a logic-level digital pattern generator such as a μ -controller or a field-programmable gate array (FPGA). Alternatively, a gate driver can be used to translate the logic-level signals to a higher voltage and/or offer a higher current driving capability to reduce the delay.

On implementation, transistors CSD17483F4 (nMOS) and CSD23382F4 (pMOS) of Texas Instruments were used along with a Xilinx Spartan-6 FPGA, clocked at 100 MHz, for the generation of the control signals.

Furthermore, the high-frequency spectrum of the control signals should be taken into consideration during the printed circuit board (PCB) design. High-speed design techniques must be used to ensure the signal integrity of the control signals.

Finally, multiple power supply decoupling capacitors with low equivalent series resistance (ESR) must be used, possibly in several locations, to stabilize power supply voltage in the transients.

III. SENSOR'S SENSITIVITY AND OFFSET AS A FUNCTION OF THE SET-RESET PULSE DURATION

The sensor has to be set-reset frequently in order to maintain correct polarization/alignment of its magnetic dipoles and has a maximum and, therefore, constant sensitivity.

Set-reset time is a *dead* time of the sensor since no measurement can be taken until the set (reset) current has been essentially zeroed, and the magnetic dipoles have been stabilized. Therefore, the total dead time depends on both duration of the set (reset) pulse and inherent settling time of the magnetic material.

In this section, the effect of the set and reset pulse duration on the sensor's sensitivity and offset is examined. The focus is not on the derivation of accurate sensitivity and offset values but on determining whether and how they change with the duration of the set-reset pulses.

The sensor's output is measured under a fixed-strength magnetic field, before, during, and after the set-reset pulses of different durations are applied. This reveals the sensor's transient behavior. Furthermore, the steady-state sensor's output voltages are measured to calculate the (steady-state) offset and sensitivity as a function of the pulse duration.

A. Experimental Setup

The experimental setup used for offset and sensitivity measurements is shown in Fig. 8. An Agilent E3631A power supply was used to provide the supply voltages for the S/R circuit, and Keithley 4200 Source Measurement Unit (SMU) was used to power the sensor bridge and capture its output. Finally, Digilent Analog Discovery 2 (based on Xilinx Spartan-6 FPGA) was used to generate the required control signals for the S/R circuit.

B. Transient Sensitivity During Set Pulses of Different Durations

The experimental setup in Fig. 8 has been used to capture the response of the sensor to set the pulses of different duration, shortly after a sequence of multiple reset pulses had been applied. The sensor's output voltage was recorded continuously, and a time subinterval starting after the sensor has been reset and ending after the following set pulse is shown in Fig. 9(a)–(c) for 40 ns, 300 ns, and 2 μ s set pulses, respectively. A constant (dc) current is applied to the offset coil as shown in Fig. 8, throughout the whole experiment, and the sensor is biased with 5 V. As shown in Fig. 9, the output of the sensor in the reset state is about

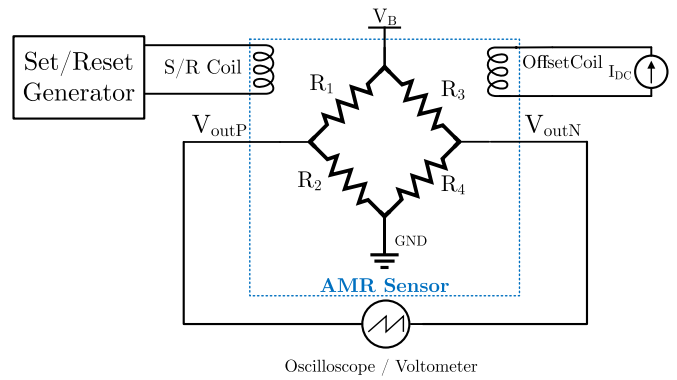


Fig. 8. Experimental setup for measuring sensor's offset and sensitivity as a function of the set (reset) pulse duration.

$V_R = -80$ mV and $V_S = 60$ mV in the set state, for all three cases. Using the manufacturer's definitions [9], equations (1), it is approximately $V_{\text{offset}} = -10$ mV and $V_{\text{field}} = 70$ mV. Moreover, in Fig. 9, it seems that the sensor's output requires at least 200 ns to settle after the set pulse current transient has been essentially zeroed, independently of the pulse duration. This, however, should be interpreted carefully: On the one hand, the traveling of the magnetoacoustic pulse along the ~ 1 mm sensing element takes about 200 ns due to the domain wall nucleation and propagation at the end of a set pulse [1], [29], [30]. On the other hand, the set current dies slowly after the pulse, requiring about the same time to become negligible.

In any case, the interesting conclusion is that the sensor can be set, settled, and achieved its maximum sensitivity in significantly less time than the several microseconds period recommended in the manufacturer's datasheet and implemented by the proposed operating circuits [9].

C. Offset and Sensitivity as a Function of Set and Reset Pulses Duration

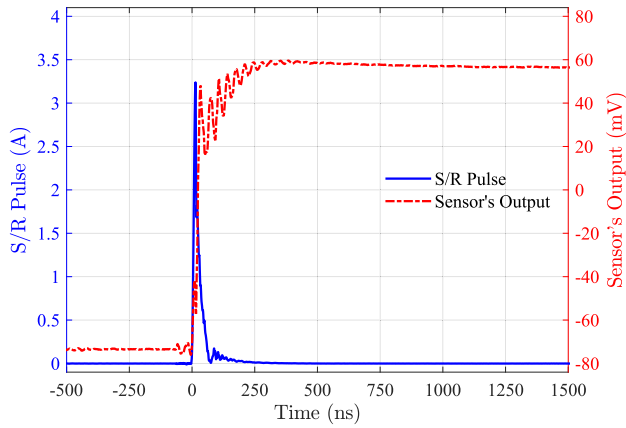
The four amorphous magnetoresistors of the sensor forming the Wheatstone bridge in Fig. 8 may have a small mismatch introducing an output offset voltage [9].

To estimate and remove the offset, the measurement scheme in Fig. 10(a) is recommended in the sensor's datasheet [9]. The magnetic field is measured twice: once after a set pulse, resulting in (steady-state) output voltage V_S , and once after a reset pulse, resulting in (steady-state) voltage V_R . Then, the output voltages, due to the offset and due to the magnetic field, are defined accordingly as

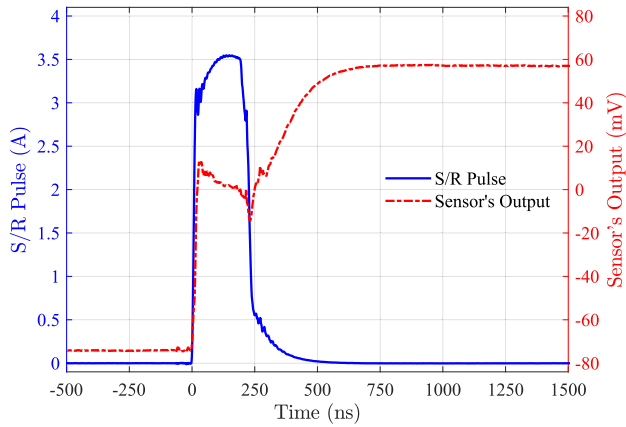
$$\begin{aligned} V_{\text{OFFSET}} &= \frac{1}{2}(V_S + V_R) \\ V_{\text{FIELD}} &= \frac{1}{2}(V_S - V_R). \end{aligned} \quad (1)$$

Assuming a fixed bridge bias voltage V_B , the *set-reset* sensitivity of the sensor, $D_{S/R}$, is defined as the linear gain of V_{FIELD} with respect to the magnetic field strength. The *set* and *reset* sensitivities are defined accordingly using V_S and V_R , respectively.

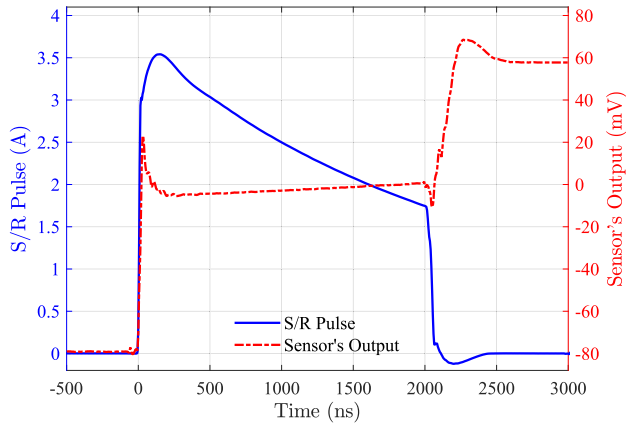
To eliminate any magnetization memory between the set and the reset states, a modification of the manufacturer's scheme,



(a)



(b)



(c)

Fig. 9. Sensor's output voltage when set pulses of different duration are applied, captured around a set pulse following a reset one. A constant (dc) current is applied to the offset coil, and the sensor is biased with 5 V. The output in the reset state is about $V_R = -80$ mV and $V_S = 60$ mV in the set state. (a) 40 ns set pulse. (b) 300 ns set pulse. (c) 2 μ s set pulse.

shown in Fig. 10(b), is preferred. Three reset pulses precede the set pulse, and similarly, three set pulses precede the reset pulse. This way, before a set or a reset pulse, the AMR sensor is in a well-defined opposite magnetization state. Therefore, the set and reset pulses of duration T_P should provide enough energy to reverse the magnetization state (180° rotation). The modification of the measurement scheme with the triple reset

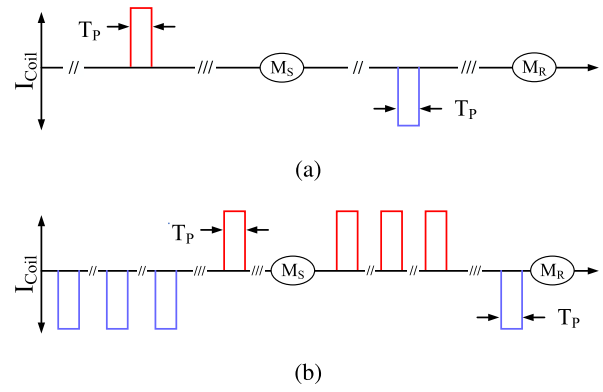


Fig. 10. AMR sensor's measurement schemes. " M_S " (" M_R ") stands for measurements after a set (reset) pulse. (a) Suggested S/R switching measuring scheme. (b) Triple S/R switching measuring scheme.

pulsing is to ensure that the sensors' magnetization state just before the set pulse is independent of the set pulse duration. Application wise, when a faster response is required, the manufacturers' recommended measurement scheme of Fig. 10(a) is appropriate.

To improve the relative accuracy of the offset and the sensitivity estimation, the sensor's readings V_S and V_R for a range of magnetic field strength were used. Specifically, for a sequence of set/reset patterns, the offset coil was excited with dc currents ranging from -100 mA up to 100 mA, resulting in a magnetic field of about -200 μ T to 200 μ T according to the sensor's datasheet [9]. Note that absolute accuracy is not important here; therefore, there was no need to generate a magnetic field with high accuracy using 3-D Helmholtz or Maxwell coils.

The output of the sensor was oversampled and appropriately filtered by the Keithley 4200 SMU. A linear regression analysis was applied to the recorded values of V_S and V_R for the different field strengths, resulting in V_{OFFSET} and V_{FIELD} estimates.

Note that the offset V_{OFFSET} and the field V_{FIELD} voltages depend on the die (chip) temperature and the bridge bias voltage; both of them must be stable during the measurements. Here, it was used $V_B = 10$ V (Fig. 8), and the ambient temperature was $T_a = 21 \pm 3$ $^\circ$ C. Furthermore, V_{OFFSET} and V_{FIELD} depend directly on the external magnetic field. Magnetic field varying between the set and reset measurements can alter V_{OFFSET} and V_{FIELD} dramatically. Even a (strong) constant field can impact the two voltages by exciting the nonlinearities of the sensing elements. Therefore, all measurements should be done in a zero Gauss chamber [31].

1) *Offset*: The offset measurements for S/R pulse duration of 40 ns to 3 μ s are shown in Fig. 11. The offset appears to be independent of the pulse duration. It changed, however, by about 0.45 mV, i.e., 1.5%, between the 1st and the 2nd days of measurements (corresponding to the small and large values of T_P , respectively); this was most probably due to small ambient temperature change.

2) *Sensitivity*: The sensitivity measurements for the set measurements (M_S), reset measurements (M_R), and the

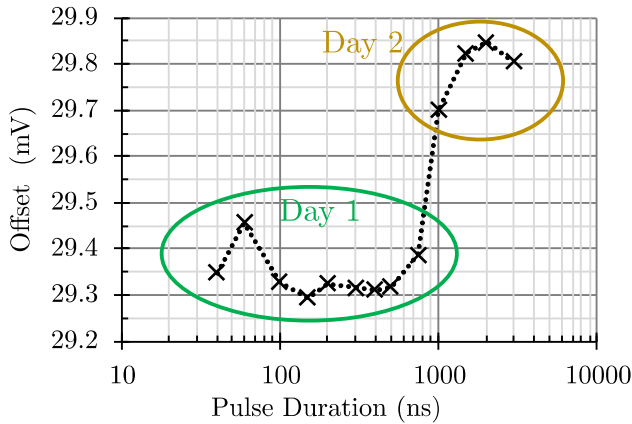


Fig. 11. Sensor's offset with $V_B = 10$ V (Fig. 8).

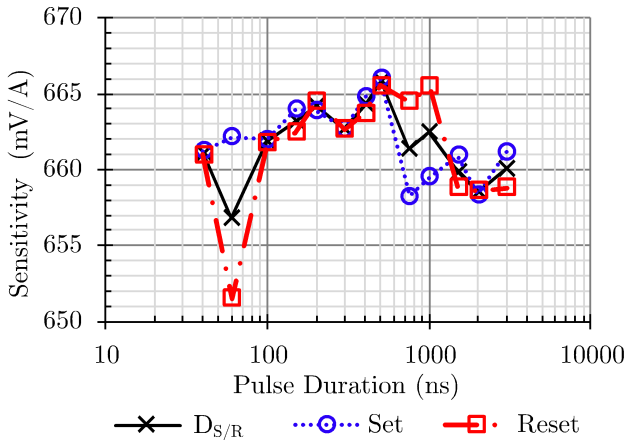


Fig. 12. Sensor's sensitivity with $V_B = 10$ V (Fig. 8).

combined S/R difference are shown in Fig. 12 for S/R pulse duration ranging from 40 ns to 3 μ s. The sensitivity variation for different S/R pulse durations is about 2%, indicating that the AMR sensor's sensitivity does not degrade, even when short S/R pulses are used.

It should be noticed that the variation in the offset and the sensitivity, across different pulse durations, is probably due to environmental factors, including magnetic field changes, magnetic shield nonidealities, and temperature variations. A partially open zero Gauss chamber was used, which was not ideal.

IV. S/R COIL POWER DISSIPATION AND SENSOR'S PACKAGE TEMPERATURE AS A FUNCTION OF S/R PULSE DURATION

The properties of the magnetic material are, in general, sensitive to the temperature and can impact the sensitivity and offset of the sensor [9]. This section estimates the power dissipated on the S/R coil, due to the S/R pulse sequence, and relates it to the steady-state temperature of the sensors package.

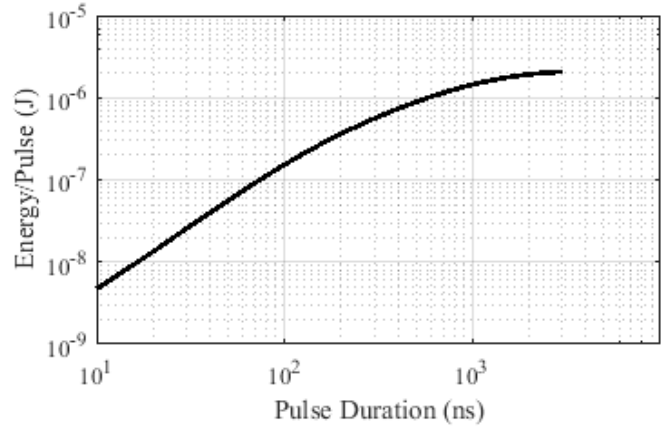


Fig. 13. Energy dissipation per pulse on the S/R coil.

Two experiments were conducted. The first one determined the energy dissipation per pulse; the second one measured the sensor's package temperature for periodic sequences of set–reset pulses with a range of frequencies and provided the package-to-ambient thermal resistance.

A. Energy Dissipation on the S/R Coil per Set and Reset Pulse

For ideal square current pulse of magnitude I_{Coil} on the S/R coil, the energy dissipated per pulse of duration T_P is $R_{Coil} I_{Coil}^2 T_P$. In a real set–reset pulse generation circuit, similar to the proposed one in Fig. 3, the current pulse is not square, and its shape is defined by several components including the dc protection capacitors C_R and C_L .

The energy dissipation per pulse on the S/R coil is calculated by integrating the instantaneous current through the S/R coil; the current is measured by inserting a 0.1 Ω resistor in series with the coil. This is done for pulse duration T_P ranging from 40 ns to 3 μ s, and the results are shown in Fig. 13.

Note that because of the symmetry of the proposed pulse generation circuit, the energy per pulse is ideally the same for both set and reset pulses.

Note also that for $T_P = 2$ μ s, which is the recommended pulse duration by the manufacturer [9], the energy dissipation per pulse is 1.92 μ J. On the contrary, the energy dissipation per pulse for $T_P = 100$ ns is only 153 nJ.

Thus, the total power consumption on the sensor as well as its thermal stress and potential temperature drift can be reduced by using shorter S/R pulses without sacrificing the sensitivity of the sensor as shown in Section III.

B. Sensor's Package Temperature and Thermal Model

The following experiment was performed to relate the S/R pulse frequency with the package temperature of the sensor. A periodic pattern of alternating set and reset pulses, following Fig. 10(a), was used. The pulse duration was $T_P = 100$ ns, and a pair of set and reset pulses (pattern) was repeated with a frequency of $f_{S/R}$.

The package temperature was measured with a thermal infrared camera (FLIR T420). Frequency $f_{S/R}$ was increased

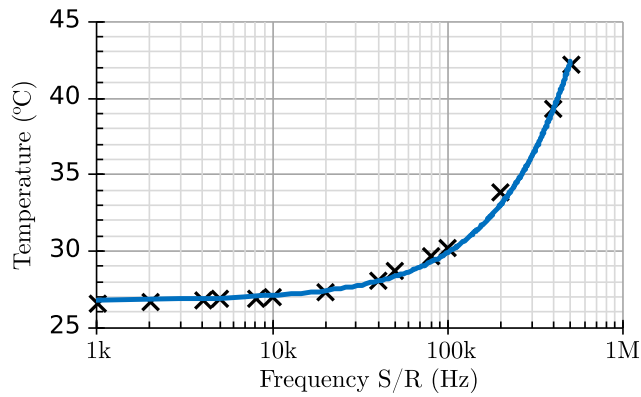


Fig. 14. Sensors temperature for various S/R pulse frequencies.

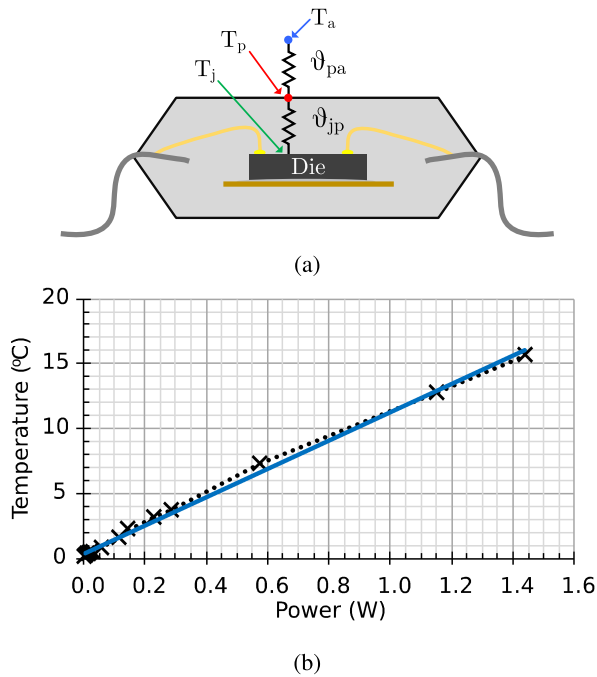


Fig. 15. HMC1001 thermal model. (a) Thermal model. (b) Sensor's temperature versus power consumption.

slowly to allow for approximate thermal equilibrium. The temperature is shown in Fig. 14. The ambient temperature was constant and about 21 °C.

Combining the measurements in Figs. 13 and 14, we can relate the (steady-state) temperature of the package with the power dissipated on the S/R coil resulting in Fig. 15. Then, the package-to-ambient thermal resistance θ_{pa} (Fig. 15) is about 10 °C/W.

V. CONCLUSION

The performance limits of an AMR sensor operating with short set–reset polarization pulses of duration down to 40 ns were explored. To do so, an improved circuit topology capable of generating agile, high-speed set–reset pulses was presented. Using it, the sensor's sensitivity, offset, power consumption, and temperature were measured using set–reset polarization pulses of different durations. The experimental results indicate

that the sensor's sensitivity and offset are not affected even when set–reset polarization pulses about the two orders of magnitude shorter than what is recommended in the literature are used. This allows for the faster magnetic field sampling and the lower power consumption significantly broadening the application space of AMR sensors.

ACKNOWLEDGMENT

The authors would like to thank Prof. E. Hristoforou, Director of the Sensors Laboratory, Department of Electrical and Computer Engineering, National Technical University of Athens, and Prof. J. Georgiou, Director of the Holistic Electronics Research Laboratory, Department of Electrical and Computer Engineering, University of Cyprus, for providing access to their laboratories and guidance during the progress of this work.

REFERENCES

- [1] D. Jiles, *Introduction to Magnetism and Magnetic Materials*, 3rd ed. Boca Raton, FL, USA: CRC Press, 2015.
- [2] J. Fraden, *Handbook of Modern Sensors: Physics, Designs, and Applications*, 4th ed. New York, NY, USA: Springer-Verlag, 2010.
- [3] P. Ripka and A. Tıpek, *Modern Sensors Handbook*. Washington, DC, USA: ISTE, 2007.
- [4] S. A. C. Harmon, M. J. Hall, S. Turner, and N. Hillier, "Characterization of magnetic sensors at the operational temperatures of industrial applications," *IEEE Trans. Magn.*, vol. 51, no. 1, pp. 1–4, Jan. 2015. [Online]. Available: <http://ieeexplore.ieee.org/document/7029220/>
- [5] A. Grosz, M. J. Haji-Sheikh, and S. C. Mukhopadhyay, *High Sensitivity Magnetometers*, vol. 19, 1st ed. Cham, Switzerland: Springer, 2017. [Online]. Available: <http://link.springer.com/10.1007/978-3-319-34070-8>
- [6] P. Ripka, *Magnetic Sensors and Magnetometers*, 1st ed. Norwood, MA, USA: Artech House, 2001. [Online]. Available: <https://us.artechhouse.com/Magnetic-Sensors-and-Magnetometers-P881.aspx>
- [7] P. Ripka, M. Tondra, J. Stokes, and R. Beech, "AC-driven AMR and GMR magnetoresistors," *Sens. Actuators A, Phys.*, vol. 76, nos. 1–3, pp. 225–230, Aug. 1999.
- [8] S. Tumanski, *Handbook of Magnetic Measurements*. Boca Raton, FL, USA: CRC Press, 2011.
- [9] Honeywell India. *1 and 2 Axis Magnetic Sensors HMC1001/1002/1021/1022*. Accessed: Jan. 2020. [Online]. Available: <https://aerospace.honeywell.com/en/learn/products/sensors/low-field-high-precision-linear-1-and-2-axis-analog-magnetic-sen>
- [10] F. Xie, R. Weiss, and R. Weigel, "Hysteresis compensation based on controlled current pulses for magnetoresistive sensors," *IEEE Trans. Ind. Electron.*, vol. 62, no. 12, pp. 7804–7809, Dec. 2015. [Online]. Available: <http://ieeexplore.ieee.org/document/7163609/>
- [11] P. Ripka, M. Janosek, M. Butta, S. W. Billingsley, and E. Wakefield, "Crossfield effect in magnetic sensors," in *Proc. IEEE Sensors*, Oct. 2009, pp. 1860–1863. [Online]. Available: <http://ieeexplore.ieee.org/document/5398405/>
- [12] V. Petrucha, V. Fura, and A. Platil, "Cross-field effect in a triaxial AMR magnetometer with vector and individual compensation of a measured magnetic field," *IEEE Trans. Magn.*, vol. 53, no. 4, pp. 1–5, Apr. 2017. [Online]. Available: <http://ieeexplore.ieee.org/document/7589024/>
- [13] H. Zhu and F. Yu, "A cross-correlation technique for vehicle detections in wireless magnetic sensor network," *IEEE Sensors J.*, vol. 16, no. 11, pp. 4484–4494, Jun. 2016. [Online]. Available: <http://ieeexplore.ieee.org/document/7395276/>
- [14] P. D. Dimitropoulos, J. N. Avaritsiotis, and E. Hristoforou, "A novel micro-fluxgate sensor based on the AMR effect of ferromagnetic film-resistors," *Sens. Actuators A, Phys.*, vol. 107, no. 3, pp. 238–247, Nov. 2003. [Online]. Available: <https://www.sciencedirect.com/science/article/pii/S0924424703003789>
- [15] K. Mohamadabadi, C. Coillot, and M. Hillion, "New compensation method for cross-axis effect for three-axis AMR sensors," *IEEE Sensors J.*, vol. 13, no. 4, pp. 1355–1362, Apr. 2013. [Online]. Available: <http://ieeexplore.ieee.org/document/6395237/>

- [16] Honeywell India. (2020). *Application Note: Handling Sensor Bridge Offset (AN212)*. [Online]. Available: <https://aerospace.honeywell.com/en/learn/products/sensors/low-field-high-precision-linear-1-and-2-axis-analog-magnetic-sen>
- [17] Honeywell. (2020). *Application Note: Set/Reset Pulse Circuits for Magnetic Sensors (AN201)*. [Online]. Available: <https://aerospace.honeywell.com/en/learn/products/sensors/low-field-high-precision-linear-1-and-2-axis-analog-magnetic-sen>
- [18] Honeywell India. (2020). *Application Note: Cross-Axis Effect (AN205)*. [Online]. Available: <https://aerospace.honeywell.com/en/learn/products/sensors/low-field-high-precision-linear-1-and-2-axis-analog-magnetic-sen>
- [19] S. Sordo-Ibanez *et al.*, "A front-end ASIC for a 3-D magnetometer for space applications by using anisotropic magnetoresistors," *IEEE Trans. Magn.*, vol. 51, no. 1, pp. 1–4, Jan. 2015. [Online]. Available: <http://ieeexplore.ieee.org/document/7029210/>
- [20] I. Georgakopoulos, N. Hadjigeorgiou, and P. P. Sotiriadis, "A CMOS closed loop AMR sensor architecture," in *Proc. Panhellenic Conf. Electron. Telecommun. (PACET)*, Nov. 2017, pp. 1–4. [Online]. Available: <http://ieeexplore.ieee.org/document/8259975/>
- [21] N. Hadjigeorgiou, E. Hristoforou, and P. P. Sotiriadis, "Closed-loop current-feedback, signal-chopped, low noise AMR sensor with high linearity," in *Proc. 6th Int. Conf. Mod. Circuits Syst. Technol. (MOCASST)*, May 2017, pp. 1–4. [Online]. Available: <http://ieeexplore.ieee.org/document/7937679/>
- [22] R. C. Dorf and R. H. Bishop, *Modern Control Systems*. London, U.K.: Pearson, 2015.
- [23] A. V. Oppenheim and R. W. Schaffer, *Discrete-Time Signal Processing*, 3rd ed. London, U.K.: Pearson, 2009.
- [24] A. V. Oppenheim, A. S. Willsky, and S. Hamid, *Signals & Systems*, 2nd ed. Upper Saddle River, NJ, USA: Prentice-Hall, 2003.
- [25] H. Witschnig, A. Morici, B. Schaffer, and J. Zimmer, "A fully monolithic integrated anisotropic magnetoresistance based angle sensor for automotive," in *Proc. 17th Int. Conf. Solid-State Sens., Actuators Microsyst. (TRANSDUCERS EUROSENSORS)*, Jun. 2013, pp. 2257–2260. [Online]. Available: <http://ieeexplore.ieee.org/document/6627254/>
- [26] E. Zimmermann, A. Verweerd, W. Glaas, A. Tillmann, and A. Kemna, "An AMR sensor-based measurement system for magneto-electrical resistivity tomography," *IEEE Sensors J.*, vol. 5, no. 2, pp. 233–241, Apr. 2005. [Online]. Available: <http://ieeexplore.ieee.org/document/1411801/>
- [27] P. Horowitz and H. Winfield, *The Art of Electronics*, 3rd ed. London, U.K.: Cambridge Univ. Press, 2015.
- [28] N. G. Hadjigeorgiou and P. P. Sotiriadis, "Parasitic capacitances, inductive coupling, and high-frequency behavior of AMR sensors," *IEEE Sensors J.*, vol. 20, no. 5, pp. 2339–2347, Mar. 2020.
- [29] D. J. Buttle *et al.*, "Magnetoacoustic and Barkhausen emission in ferromagnetic materials," *Phil. Trans. Roy. Soc. A, Math., Phys. Eng. Sci.*, vol. 320, no. 1554, pp. 363–378, Nov. 1986. [Online]. Available: <http://rsta.royalsocietypublishing.org/cgi/doi/10.1098/rsta.1986.0124>
- [30] J. J. Quinn, "Theory of the parallel field magnetoacoustic effect," *Phys. Rev. Lett.*, vol. 11, no. 7, pp. 316–318, Oct. 1963. [Online]. Available: <https://link.aps.org/doi/10.1103/PhysRevLett.11.316>
- [31] S. Angelopoulos, P. Vourna, A. Ktena, P. Tsarabaris, and E. Hristoforou, "Design and development of a new magnetometer calibration device," *IEEE Trans. Magn.*, vol. 55, no. 1, pp. 1–4, Jan. 2019.